X-RAYS USING ULTRA INTENSE LASERS FOR EFFECTIVE THERANOSTICS

Sultana N. Nahar

Department of Astronomy, The Ohio State University, Columbus, OH 43210, USA
E-mail: nahar@astronomy.ohio-state.edu

Advent of portable monochromatic x-ray lasers is eagerly awaited as it will enable a big step toward advances in many technological applications, particularly for more precise treatment of cancer. X-rays are most widely used in the medical field, especially for diagnostics and therapeutics (theranostics) of cancer. However, the current medical x-ray sources are based on the old technology of x-ray tubes and lack in specificity in the emitted energy and produce broadband bremsstrahlung radiation. In addition, very high energy x-ray photons in the MeV range from LINACs are commonly used for irradiating the patient in order to obtain high intensity at sufficient tissue depth. This is highly inefficient since the low-energy x-rays in the bremsstrahlung spectrum are absorbed without significant penetration into the body, and thus cause burn, and the high energy x-rays pass through without much interaction with the radiosensitizing agents, and thus break healthy tissues. Study using our proposed method "Resonant Nano-Plasma Theranostics" (RNPT) for cancer treatment shows that the most effective x-ray energy range for malignant cell destruction, using high Z radio-sensitizing agents, lies within 100 keV energy region of the bremsstrahlung. Hence, an appropriately tuned monoenergetic x-ray source of sufficient intensity falls under the proper energy range and is highly desirable for theranostics. Through RNPT, we were also able to demonstrate production of monochromatic x-rays from bremsstrahlung radiation of a x-ray source.

It is known that ultra intense laser solid interactions produce copious amounts of x-rays, both monoenergetic K_α photons and a bremsstrahlung. Through couplings of the laser field and electron energy, the intense laser field initiates multiple ionization of the the matter. The highly energetic electrons produce x-rays by ejecting other inner-shell electrons and bremsstrahlung by colliding with the nuclei. If the monochromatic radiation can be maximized and is made tunable to resonant photon absorption energies of the heavy nanoparticles in nanobiomedicine, a safest and most effective treatment can be achieved.

RNPT predicts the resonant energies and corresponding x-ray emissions, particularly K_α photons, from various ionization states, such as from hydrogen to fluorine-like states, of high Z elements in radio-sensitizing agents. Such studies have been carried out for a number of elements, such as, gold, platinum, lead, uranium etc. Interestingly the Berkeley group has recently detected such emission of K_α photons at resonant energies of various ionization states of aluminum in warm dense plasma state using a x-ray free electron laser (XFEL). These issues are elaborated in regard to RNPT.

Keywords: X-rays from high Z element, K_α transitions, laser-matter interaction, x-ray resonant fluorescence; photoinization; Cancer therapy and diagnostics

1. Introduction

Cancer is a disease that is affecting people all over the world. Only a fraction of its various types can be cured. It is imperative to find ways to cure the disease. Most of the current treatments incur additional side effects. Treatments such as chemotherapy causes cytotoxicity and radiation therapy causes burn and damage of tissues. A monochromatic x-ray laser can play a crucial role for a more precise treatment for diagnostics and therapy for cancer patients.

It has been found that x-rays along with nanoparticle (NP) radiosensitizer embedded in a cancerous tumor yields more effective cure than irradiation of x-rays alone. Heavy elements nanoparticles can absorb or emit high energy x-rays and hence are commonly implemented in radio-sensitizing agents. For example, with gold NP, less radiation was needed to kill the defective cells in mice experiment than that in radiation therapy (e.g.,[1]). The 30 days experiment showed that x-ray irradiation with AuNP reduced 85% of the tumor volume. A monochromatic x-ray source, created through a laser, should be more effective since it can be matched to resonant absorption of the NPs and thus can give accurate dosemetry.

2. Resonant Nano-Plasma Theranostics (RNPT)

Our proposed method, *Resonant Nano-Plasma Theranostics*,[2–5] as described in Fig. 1, focuses on monochromatic x-ray spectroscopy of nanoparticles rather than broad band imaging and therapy. As shown in Fig. 1, a cancerous tumor is embedded with high Z (HZ) nanoparticles (NP). To avoid damage of body tissues from irradiation, the NP should be of elements heavier than the biogenic elements, such
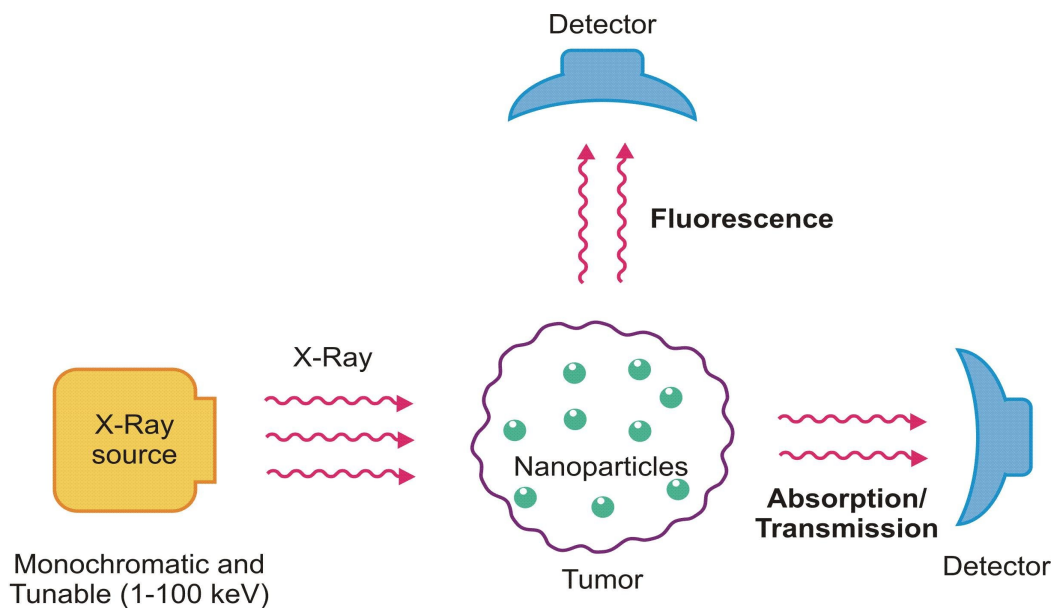
Fig. 1.   RNPT method where monochromatic x-rays are targeted at the resonant energy of the nanoparticles embedded in the tumor. The aim is to initiate Auger cascades following K-shell ionization of the high z element in the nanoparticles

as, H, O, C, K, Fe etc, such that the high energy X-rays interact with only with them. The figure shows a monochromatic X-ray source is directed to the tumor for inner shell, mainly K-shell, ionization of the NPs. The x-ray energy is tuned to the resonant energy of the HZ element for maximum absorption. The purpose is initiate fluorescent emission and ejection of electrons that can create in vitro a nano-plasma. The ejected electrons which are at ∼keV energy range can have penetration depth of nm range. These will attach and breakup the DNAs of the surrounding malignant cells. The fluorescent emission can be used for imaging. Hence, both the electrons and photons are used for the therapy and diagnostics or *theranostics*. Hence spectroscopically targeted resonant x-rays, produced by an intense laser, should reduce the exposure by precise energies and be far more efficient in cell destruction and cure. At low intensity the x-ray source can produce high quality narrow band K_α imaging. and at high intensities may cause more cell destruction.

3. X-ray Interaction with Elements

The two radiative processes that occur due to x-ray absorption by an element are photoexcitation (inverse is de-excitation) and photoionization (inverse is electron-ion recombination). In photoexcitation an electron is excited to a higher energy level,

$$X^{+z} + h\nu \rightarrow X^{+z*}$$
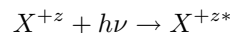
but remains bound with the ion. The asterisk (*) denotes an excited state. Its strength is determined by the oscillator strength (f). The atomic parameter for de-excitation is the radiative decay rate or Einsteins A-coefficient. In photoionization an electron is energetic enough to be free, that is, go to continuum:

$$X^{+z} + h\nu \rightarrow X^{+z+1} + e$$
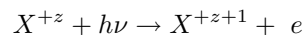
This direct ionization gives the background feature of the process. Photoionization can also occur via an intermediate doubly excited autoionizing state as described below where an electron collides with an ion and forms a doubly excited (double asterisks) autoionizing state.

$$e + X^{+z} \rightleftharpoons (X^{+z-1})^{**} \rightleftharpoons \begin{cases} e + X^{+z} & \text{AI} \\ X^{+z-1} + h\nu & \text{DR} \end{cases}$$
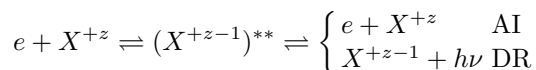
The autoionizing state leads either to autoionization (AI) when the electron goes free or dielectronic recombination (DR) when a photon is emitted as the electron combines with the ion. The inverse of DR is photoionization. The photoionization cross section is designated by σ_{PI}. This two-step process introduces a resonance in the cross section.

The oscillator strengths and photoionization cross sections can be obtained from the generalized

line strengths as (e.g.[6]),

$$\mathbf{S} = \left| \left\langle \mathbf{\Psi_f} | \sum_{\mathbf{j=1}}^{\mathbf{N}} \mathbf{r_j} | \mathbf{\Psi_i} \right\rangle \right|^{\mathbf{2}}. \tag{1}$$

where Ψ_i and Ψ_f are the initial final state wave functions. For oscillator strengths (f_{ij}), the final wave function is bound while for photoionization cross sections (σ_{PI}), it is a continuum. f_{ij}, σ_{PI} and the mass attenuation coefficients κ can be obtained from generalized line strength as

$$f_{ij} = \left[\frac{E_{ji}}{3g_i} \right] S, \; A_{ji}(sec^{-1}) = \left[0.8032 \times 10^{10} \frac{E_{ji}^3}{3g_j} \right] S,$$

$$\sigma_{PI}(K\alpha, \nu) = \frac{4\pi^2 a_o^2 \alpha}{3} \frac{E_{ij}}{g_k} S,$$

$$\kappa(\nu; K\alpha) = \frac{\sigma_{PI}(\nu; K\alpha)}{u W_A}. \tag{2}$$

where u is 1 amu=1.66054e-24 g and W_A is atomic weight.

4. Auger Process Through Photoionization

X-rays with energies higher than K-shell ionization energy of the HZ element in the nanoparticle can photoionize element with creation of a hole in the 1s shell. As shown in Fig. 2, the hole is filled up by dropping of a L-shell electron when the excess energy of the electron is emitted as a photon. This filling of inner-shell hole with emission of a photon is known as the Auger process. The emitted photon can knock out another L-shell e^- and can ultimately create two holes in L-shell. The two vacancies in the L-shell are to be filled by two M-shell e^-s. The process can lead to cascade of electron and photon emissions as multiple vacancies move upward. The cascade effect is referred to as Coster-Kronig or Super-Coster-Kronig cascade (e.g.[6]). Hence a single ionization of 1s electron can lead to ejection of 20 or more electrons in an ion with occupied O and P shells.

The number of electron emissions depends on the radiative decay rates or Einstein's A-coefficients as well and hence there may be more of one ionization state than the others. Typically K-L transitions (K_α transitions) have the highest probabilities or A-values and show as high peak resonances in the photoionization cross sections. An external source with

energy equal to K-L transition can be introduced to compete with the downward decays. Then the resonant excitation from the K-shell into electron vacancies in higher L-shell can result in considerable increment in ejection of electrons. For any two-level system $i \leftrightarrow j$ and transition frequency ν and radiation field density $\rho_{ij}(\nu)$, the incident photon flux Φ at the resonant energy of $K\alpha$ should be greater than the critical flux,[3]

$$\Phi^c(\nu_{K\alpha}) = \frac{\sum_{n_i > 2} g_i A[n_i(S_i L_i J_i) \rightarrow 2(SLJ)]}{g_K B_{K\alpha}}. \tag{3}$$

where $n_i(S_i L_i J_i)$ refers to specific fine structure levels of an n-shell, e.g. $2(S_i L_i J_i)$ refers to the L-shell levels.

5. Photoionization and Dose Deposition of Pt

Photoionization shows characteristic features when the photon energy reaches that of a shell threshold. The cross section σ_{PI} is enhanced at the ionization threshold as seen in Fig. 3. The figure shows rises in photoionization of platinum nanoparticles (PtNP) at M-, L- and K-shell ionization. The rise at K-shell ionization edge is at about ~ 78 keV. As discussed earlier, the values of photoionization and photoabsorption coefficient are the same except for a constant. K-shell ionization of high Z nanoparticles have been the focus for enhancement of electron ejections, but without success. The reason is the low cross sections K-edge compared to that at lower energy. RNPT predicts resonant energy for platinum at about 65-69 keV, below the K-edge, where probability of electron production is orders of magnitude higher than that at K-edge, shown in red in Fig. 3.[7] These resonances were computed separately and added to the background cross section.

Dose Enhancement Factor (DEF) is a important quantity in radiation therapy that gives a measure of radiation absorption in tissues for treatment with and without a radiosensitizing reagent. Fig. 4 presents Monte Carlo simulation of radiation dose deposition in tissues for x-ray absorption at three different energies, 100 keV, 170 keV, 6 MeV from three broadband X-ray sources.[8] The 1st peak($\sim$40 keV) in all three curvres is due to L-shell ionization, 2nd peak (~ 80 keV) is due to K-shell ionization. Beyond K-edge, DEF decreases as there is no other threshold beyond it. The figure shows that DEF is con-

4
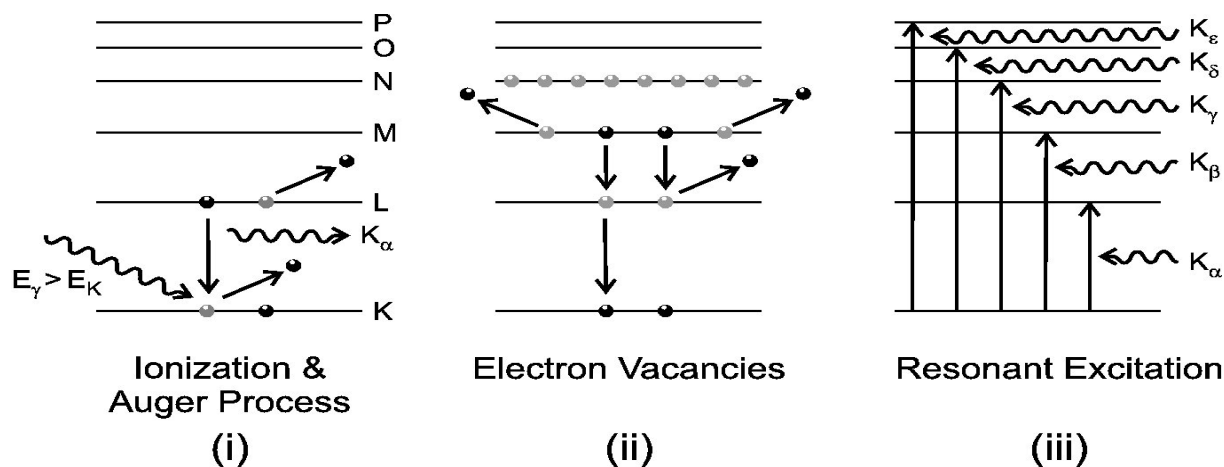
Fig. 2.   i) Auger process, ii) Koster-Kronig cascade, iii) inverse of Auger process

.
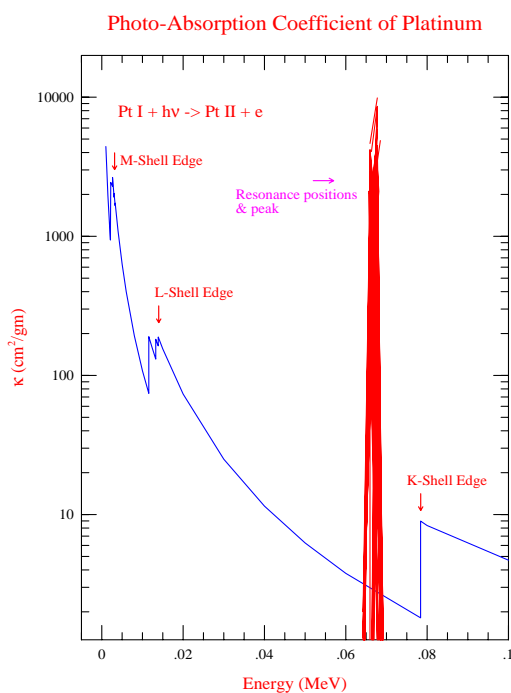
Fig. 3.   Photoionization absorption coefficient κ of neutral platinum. The background cross section shows rises at M-, L-, K-shell thresholds. The energy and peaks of resonances due to inner K-shell excitations are shown in red.[7]

stant beyond 250 keV (inset, bottom panel) where the radiation is largely Compton scattered. In this simulation, the resonant effects were not considered. At about 100 keV X-rays are efficient in achieving the required DEF. Reason for exploring a keV range

X-ray source is to find high intensity laser produced plasma.
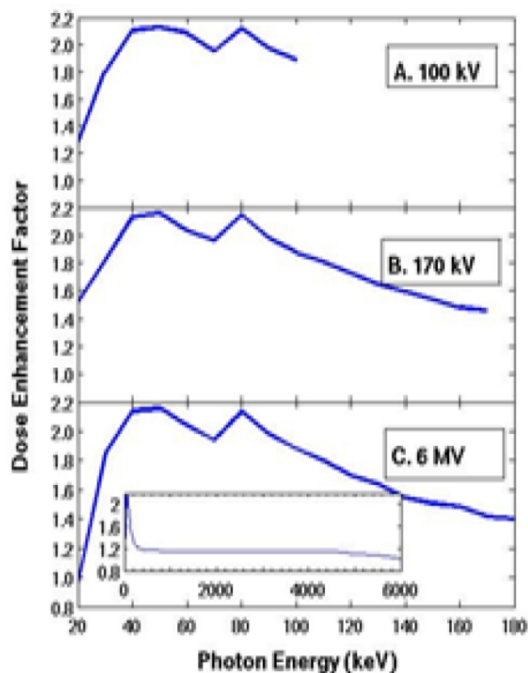
Fig. 4.   The radiation dose deposition in tissues for x-ray absorption at three different energies, 100, 170, and 6 MeV from three x-ray sources.

We studied X-ray absorptions and intensities of emitted photons and electrons by Auger process in

tissues using κ values of gold NP including the resonances in Monte Carlo simulation.[?] The K_α resonances of AuNp lie around 68 keV. We found that at lower concentration of AuNP contrast agent, the DEF to be an order of magnitude greater at gold $K\alpha$ resonant energy than those at K-shell ionization energy at 82 keV and at 2 MeV, the peak voltage of a linear accelerator or LINAC energy of 6 MeV. It may be noted that K-shell ionization energy of all elements are within 100 keV. Hence these findings show that most of x-ray photons generated at the x-ray sources are ineffective for the treatment.

6. X-Rar Sources in Medical Facilities

As mentioned above, most of the x-ray sources in medical
facilities produce broadband bremsstrahlung radiation. The energy range of a typical bremsstrahlung of an element varies from 0 to the peak voltage of the machine. Fig. 5 shows a typical x-ray set-up in medical facilities and the inset gives a schematic diagram for radiation production. A beam of electrons is accelerated across the voltage difference ΔV between the cathode and the anode, strikes a high-Z target (e.g. tungsten W with Z=74), produces the bremsstrahlung as they decelerate. Among the typical x-ray sources, the high energy linear accelerators or LINACs produce the peak energy ranging from 6 MeV to 10-15 MVp, and the lower energy machines such as CATScanners produce the peak energy going up to 100-250 KVp

The top panel of Fig. 6 shows bremsstrahlung of tungsten (squares) from a 100 V machine. The low energy x-rays are filtered out as they cause harm to tissues. The panel shows the filtering by commonly used aluminum filter (dotted). Hence the resultant radiation curve shows a broad feature with a maximum at $\sim 1/3$ of the kVP or MVp. The bottom panel shows bremsstrahlung of a 6 MeVp LINAC where the low energy x-rays have been filtered out. Only a fraction, around the peak region in the lower energy below 250keV, of the bremsstrahlung is absorbed for effective theramostics.

7. X-Rays From Ultra Intense Laser Matter Interaction

It is known that the strong fields of ultra intense short pulse (10^{17-19} W/cm^2) laser can cause instant
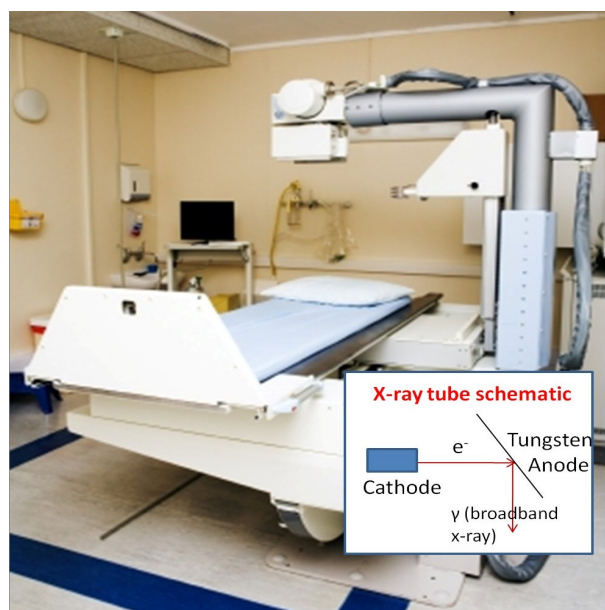
Fig. 5.   Typical x-ray machine in a medical facility. The inset shows diagram of production of x-rays

multiple ionization of atoms in a solid placed in the laser focus. Ionization is initiated in all forms of matter above 10^{14} W/cm^2 intensity with typical laser wave length of 1 μm via multi-photon absorptions and then tunnel ionization process. Single photon ionization of materials requires the interaction of photons with energy at and beyond the binding energy of the electron. However, in a high photon density field, a bound electron absorbs multiple lower energy photons to overcome its potential well and ionize. Hence with high laser electric field, the photon energy becomes largely irrelevant.

The ionization occurs through electric field stripping of the individual atoms electrons in the material. This mechanism has been experimentally verified up to 10^{20} Wcm^{-2}. The ejected electrons are highly energetic. For example, at intensity of 10^{16} W/cm^2, the electrons can reach an energy of several keV. These electrons collide with the matter at near light speed within a fraction of an optical cycle. The interaction among the electrons and light field coupled together to create a state of matter called High Energy Density (HED) plasma (density 10^{12-13}) for typical focal spot of a few micron diameter. The highly complex behavior of such plasma gives rise to many fascinating phenomena like GeV electron acceleration, MeV ion acceleration and nuclear fusion. However, it also produces a characteris-

6
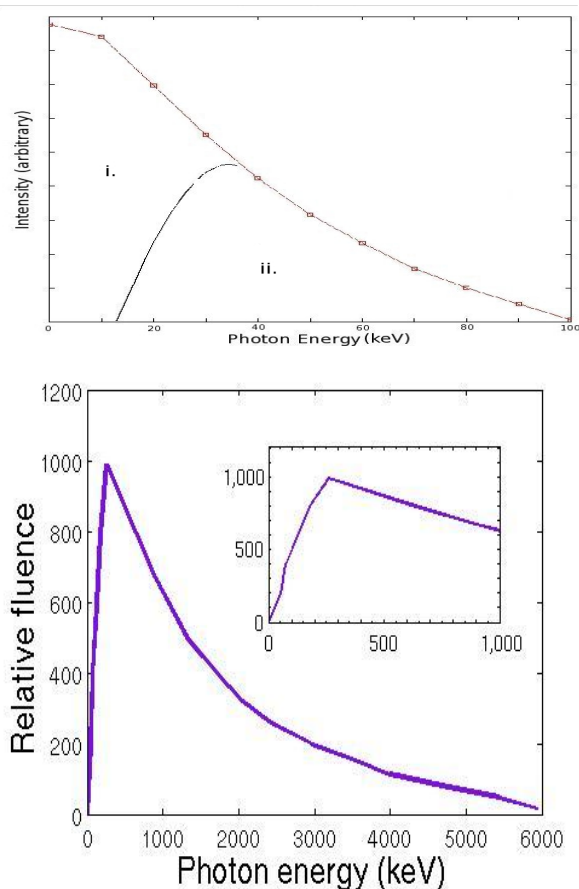
Fig. 6.   Bremsstrahlung from, a 100 keV (top panel) X-ray source and a 6 Mev LINAC (bottom) with a peak around 35 keV and 300 keV, respectively, after filtering out the lower energy x-rays

tic x-ray line emission (e.g. K_α), and a broad-band background bremmstrahlung X-ray radiation.

The K_α radiation is produced as highly energetic electrons collide with atomic nuclei and knock out K-electrons when directed by various mechanisms such as, Brunel heating (p-polarized light) and **jxB** Lorentz force (forward motion) heating. The bremsstrahlung is produced as the energetic electrons collide with the nuclei. An important fact of these radiation is that the K_α emission is isotropic, whereas the bremsstrahlung emission is strongly peaked in a cone around the laser k axis (due to MeV electron forward motion).

OSU (Ohio State University) Project is a proposed plan that aims to maximize the K_α emission and minimize bremmstrahlung emission to create a next generation mono-chromatic x-ray source for biomedical radiography, imaging and potential cancer treatment application. One major issue involves ca-

pability of reliably reaching the intensity by an Ultra Intense Laser and effort to maintain the prepulse to main pulse contrast and the spatio temporal shape over a period of experimental effort. The OSU team has already achieved such laser system with multiple repetition rate (from kHz -10 Hz to single shot), intensity range (10^{1420} W/cm^2) and pulse contrast (10^{-10}:1) ratio. The development of such an ultraintense laser initiated x-ray (ULIX) source will require careful optimization of Laser plasma interaction (LPI) parameter space.

It has been reported that x-ray energies could be up to MeV in bremsstrahlung from laser plasma electrons in high Z targets and at laser intensities 10^{15-17} W/cm2, and increase in x-ray yield with laser matter interaction with sub-wavelength scale structures on target surfaces. Park et al (2004[9] showed that laser energy to Ag K_α conversion efficiency up to 0.01% at laser intensity of 10^{18} or higher. Fig. 7 presents x-ray conversion efficiencies from some ultra intense laser systems. It was found that laser energy absorption can be increased up to ∼95% at low intensity by changing target surface morphology.
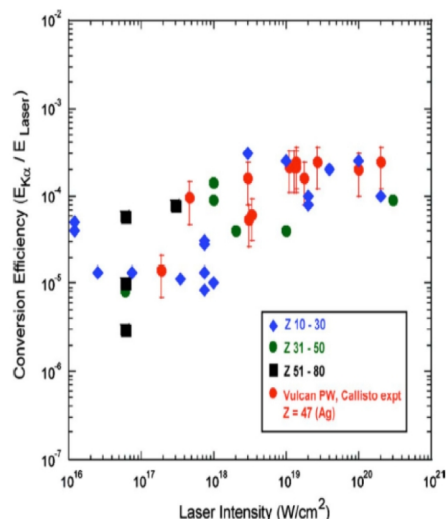
Fig. 7.   Absolute conversion efficient vs laser intensity.[9]

8. Production of Monochromatic X-rays

Under RNPT study, it has been shown that monochromatic x-rays can be produced from

bremsstrahlug radiation.[8] Bremsstrahlung from a 100 keV x-ray source was directed to a Zr-plate positioned at a particular angle. Inner K-shell ionization in the target followed by radiative decays by upper shell e$^-$s led to X-ray fluorescence at monochromatic energies, as seen in Fig. 8. The top panel of Fig. 8 shows the Zr K$_\alpha$ line and a lower peak K$_\beta$ line above the scattered background; the isolated features after subtracting the background noise are shown in the bottom panel. It may be assumed, to a good approximation, that each K-shell ionization leads to the production of a K$_\alpha$ photon. The K$_\alpha$ fluorescence yield may be expressed as

$$\omega_K = \frac{A_r(L-K)}{A_r(L-K) + A_a(L)}, \qquad (4)$$

where A_r and A_a are the radiative and autoionization decay rates respectively. The intensity of the
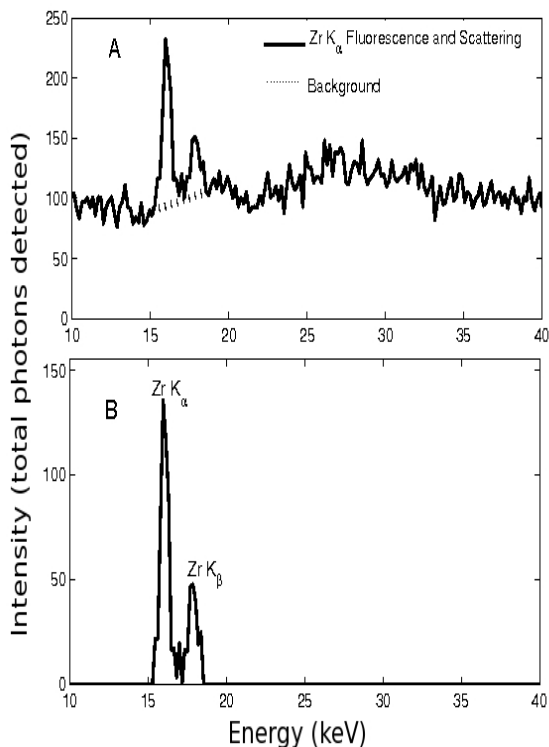
Fig. 8.   Production of K$_\alpha$ X-rays from Zr using 100 keV bremsstrahlung[?]

monochromatic energy produced can be estimated from

$$I(K_\alpha) \sim N(X) \int_{E \geq E_K}^{E(kVp)} f_B \sigma_K(E) dE$$

where f_B is the bremsstrahlung distribution function, $N(X)$ is the number density, and σ_K is K-shell photoionization cross section. For Zr the efficiency of conversion found to be $\sim 2\%$.

The K$_\alpha$ fluorescence in general produces weaker beam intensity. However, for high-Z elements the fluorescence yield, $\omega_{\mathbf{K}} > \mathbf{0.95}$. Hence all photons from the Bremsstrahlung source above the K-shell ionization energy, with E $> E_K$, may be *converted* into monochromatic K$_\alpha$ radiation with high efficiency.

9. Resonant K$_\alpha$ Emission From Hot Dense Al Plasma Using LCLS

The x-ray producing lasers are mainly the free electron lasers. They can be varied for x-ray energies by varying the voltage. These are expensive and large for medical facilities. However, x-ray free electron lasers (XFEL) produces monochromatic radiation and of these, the linear coherent light source (LCLS) can produce high intensity radiation.

One main part of RNPT method is to determine the location and use of the K$_\alpha$ resonant photoionization leading to enhanced fluorescence and electron emissions (e.g. for gold[3,10]). In recent experiments, such resonant fluorescence were detected for neon and aluminum using XFEL at SLAC (Stanford Linear Accelerator). Vinko et al at Berekely[11] created hot, over a million K, dense aluminum ($\sim$ 100 eV, solid density) isochorically heated using an intense 80 fs x-ray pulse (10^{17} W/cm^2) from soft x-ray LCLS. The photon energy was in the range of 1.56-1.83 keV, above the K-edge of Al. Due to a long penetration depth of x-ray, a bulk of hot dense matter with well defined temperature and density was possible to be created.

With FEL photon energy above the K-edge, the photoionization of a core electron is followed by the Auger decay and initiates the major ionization process at the beginning of the interaction. However, as temperature increases the collision dominates the dynamics and determines the charge state distribution of the hot dense matter. Vinko et al. found that when the FEL photon energy was below the K-end and set to K-L transitions, the multiphoton ionization channel was unveiled and the 1s-2p resonance was driven. They measured enhanced fluorescence at different energies of the various ionization states of Al. Such fluorescence occur due to resonant photoionization or the photoabsorption coefficient of various ionization

8

states of Al as shown theoretically in Fig. 9.[12] The figure shows enhancement in photoionization at resonant positions, marked by arrows, of various ionization states of Al. Vinke et al. also observed increased K_α fluorescence with higher ionization states as the theory predicts in Fig. 9. The background κ (in blue) is also shown in the figure. It shows an enhanced ionization at K-shell ionization threshold of Al. This K-shell threshold energy varies with various ionization states, such as, from 1.56 keV of neutral Al to 2.304 keV of hydrogen like Al. Vinko et al reported that modifications of emission line shape in their model indicated that the x-ray driven resonant transition of inner shell electron modified the radiative and the Auger decay processes.[12]
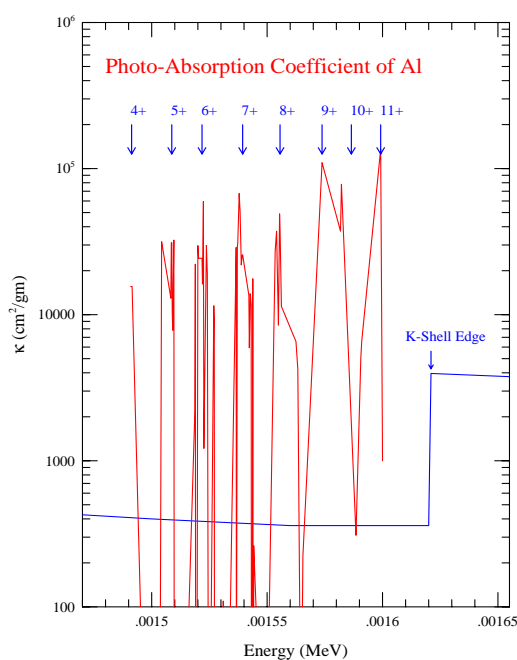
Fig. 9. Resonant $K_|\alpha$ absorption coefficients of various ionization states of aluminum, from Al^{4+} to Al^{11+}. The background (blue) shows an enhancement at K-shell ionization, however, but much lower than the resonant peaks. Vinko et al.[11] measured enhanced fluorescence at these resonant energies of Al.

10. X-Ray Lasers

Althogh LCLS is capable of high intensity coherent x-rays, there are some limitations for their us-

age at medical facilities in addition to cost and size of the set-up. The intensity (e.g. 10^{17-19} W/cm^2) of a LCLS is much higher than that needed for use in vivo nanoparticles breakdown in tissues. The energy of the emitted x-rays can be varied by varying the energies of the accelerator voltage, but it is limited to photon energies up to 8 keV at SLAC and higher at ALS at Argonne National Lab. However for high Z elements of interest require much higher energy x-rays.

A possible solution for production of monochromatic x-rays of range up to 100 keV perhaps be of accelerator-laser produced x-rays. In this setup, whose technology was developed over a decade ago, the electron beam of an accelerator is collided by infra-red laser photons positioned at right angle. Through inverse Compton scattering, the photons gain energies from the electrons and produce monochromatic x-rays along the electron beam direction. The x-ray energy can be raised near 100 keV needed for all practical purposes of theranosties. However, due to Thompson scattering of a photon with a free electron, the cross section is small and hence the intensity could be low. Investigations are in progress in various laboratories for technologies to attain the proper monochromatic x-ray source.

11. Conclusion

RNPT method for cancer treatment and the needed x-ray lasers for monochromatic radiation tuned to resonant energies of radiological sensitizing agents are presented. One important aspect of observing, using x-ray electron laser LCSL, the enhancement of fluorescence at K-L resonant energies of various ionization states of Al as predicted by RNPT is illustrated. The need for laser technologies for the needed x-rays at medical facilities is discussed. Development of various components of RNPT is in progress.

12. Acknowledgment

References

1. J. Hainfeld *et al.*, *Phys. Med. Biol.* **49**, N309 (2004)
2. A.K. Pradhan *et al.*, *The Radiotherapy Dynamics (XVth Int. Conf. Use of Comput. in Radiat. Ther.) Vol.* **2**, 89 (2007)

3. A.K. Pradhan, S.N. Nahar, M. Montenegro *et al.*, *J. Phys. Chem.* A **113**, 12356 (2009)
4. M. Montenegro, S.N. Nahar, A.K. Pradhan *et al.*, *J. Phys. Chem.* A **113**, 12364 (2009)
5. S.N. Nahar, A.K. Pradhan, M. Montenegro, in *Simulations in Nanobiotechnology*, CRC Press - Taylor & Francis Group (Ed. Kilho Eom, 2011), p.305-330
6. A.K. Pradhan and S.N. Nahar, *Atomic Astrophysics and Spectroscopy* (Cambridge University Press, 2011).
7. S.N. Nahar, A.K. Pradhan, S. Lim, Can. J. Phys. 89, 483-494 (2011)
8. S. Lim, M. Montenegro, A.K. Pradhan, S.N. Nahar, E. Chowdhury and Y. Yu, in *World Congress on Medical Physics and Biomedical Engineering IFMBE Proceedings 39*, pp. 2248-2251 (Ed. M. Long, Springer, 2012)
9. Park, H. G. et al. Science 305, 14441447 (2004)
10. S.N. Nahar, A.K. Pradhan, C. Sur, *J. Quant. Spec. Rad. Transfer* **109**, 1951 (2008)
11. S.M. Vinko et al. Nature Lett. 482, 59-63 (2012)
12. S.N. Nahar and A.K. Pradhan (in preparation 2012)